DEVELOPMENT OF A NEXT-GENERATION ENVIRONMENTAL CHAMBER FACILITY FOR CHEMICAL MECHANISM AND VOC REACTIVITY RESEARCH

Final Report to the

United States Environmental Protection Agency
Cooperative Agreement CR 827331-01-0

By

William P. L. Carter, Dennis R. Fitz, David R. Cocker, III, Irina L. Malkina,
Kurt Bumiller, Claudia G. Sauer, John T. Pisano, Charles Bufalino, and Chen Song

June 27, 2005

Center for Environmental Research and Technology
College of Engineering
University of California
Riverside, California 92521

ABSTRACT

A new state-of-the-art indoor environmental chamber facility for the study of atmospheric processes leading to the formation of ozone and secondary organic aerosol (SOA) has been constructed and characterized. The chamber is designed for atmospheric chemical mechanism evaluation at low reactant concentrations under well-controlled environmental conditions. It consists of two collapsible 90 m^3 FEP Teflon film reactors on pressure-controlled moveable frameworks inside a temperature-controlled enclosure flushed with purified air. Solar radiation is simulated with either a 200 kW Argon arc lamp or multiple blacklamps. Results of initial characterization experiments, all carried out under dry conditions, concerning NO_x and formaldehyde offgasing, radical sources, particle loss rates, and background PM formation are described. Results of initial single organic - NO_x and simplified ambient surrogate - NO_x experiments to demonstrate the utility of the facility for mechanism evaluation under low NO_x conditions are summarized and compared with the predictions of the SAPRC-99 chemical mechanism. Overall, the results of the initial characterization and evaluation indicate that this new environmental chamber can provide high quality mechanism evaluation data for experiments with NO_x levels as low as ~2 ppb, though the results indicate some problems with the gas-phase mechanism that need further study. Initial evaluation experiments for SOA formation, also carried out under dry conditions, indicate that the chamber can provide high quality secondary aerosol formation data at relatively low hydrocarbon concentrations.

ACKNOWLEDGEMENTS AND DISCLAIMERS

TABLE OF CONTENTS

LIST OF TABLES

LIST OF FIGURES

v

INTRODUCTION

Environmental chambers have been used for the past few decades to investigate processes leading to secondary pollutant formation such as ozone (Jeffries et al, 1982; 1985a-c; 1990; Gery et al, 1988; Hess et al, 1992; Simonaitis and Bailey, 1995; Simonaitis et al, 1997; Carter et al, 1995a; Carter, 2000; Dodge, 2000 and references therein) and secondary organic aerosol (SOA). (e.g., Odum et al., 1996, 1997; ; Griffin et al., 1999; Kleindienst et al., 1999; Barnes and Sidebottom, 2000; Cocker et al. 2001a-c; Jang and Kamens, 2001; Seinfeld and Pankow, 2003 and references therein, Johnson et al, 2004, Montserrat et al, 2005). These chambers are essential for developing and evaluating chemical mechanisms or models for predicting the formation of secondary pollutants in the absence of uncertainties associated with emissions, meteorology, and mixing effects. Existing chambers have been used to develop the models now used to predict ozone formation (Gery et al, 1988; Stockwell et al, 1990; Carter, 2000; Dodge, 2000 and references therein), and are beginning to provide data concerning formation of SOA (e.g., Pandis et al., 1992; Griffin et al., 2001; Pun et al., 2003; Griffin et al., 2003, Johnson et al, 2004, Montserrat et al, 2005). However, environmental chambers are not without uncertainties in characterization and variability and background effects (Carter et al, 1982; Carter and Lurmann, 1991; Jeffries et al, 1992; Carter et al, 1995a; Dodge, 2000). This limits the utility of the data and the range of conditions under which the models or mechanisms can be reliably evaluated.

For example, because of background effects and analytical limitations, most chamber experiments to date have been conducted using levels of NO_x and other pollutants that are significantly higher than those that currently occur in most urban and rural areas (Dodge, 2000). Even lower ambient NO_x conditions are expected as we approach eventual attainment of the air quality standards. The nature of the radical and NO_x cycles and the distribution of VOC oxidation products change as absolute levels of NO_x are reduced. Because of this, one cannot necessarily be assured that the current mechanisms developed to simulate results of relatively high concentration experiments will satisfactorily simulate downwind or cleaner environments.

Background effects can be minimized by using large volume reactors and assuring that the matrix air is adequately purified, that appropriate wall material is utilized, and that steps are taken to minimize introduction of ambient pollutants due to leaks or permeation. Large volume is also required for minimizing wall losses of aerosols or semi-volatile aerosol precursors, which is important in studies of SOA formation. For this reason, until recently, most studies of SOA formation have been carried out in large outdoor chambers (e.g., Jaoui et al., 2004; Griffin et al., 1999, Montserrat et al, 2005). However, outdoor chambers have diurnal, daily and seasonal changes in temperature and actinic flux, which can increase uncertainties in characterization of run conditions for model evaluation and make systematic studies of temperature and humidity effects difficult. Recently a new indoor chamber was developed to address these concerns (Cocker et al, 2001a), but that chamber was not designed to conduct experiments characterized for low pollutant conditions, and the blacklight light source employed does not represent that of natural sunlight in the longer wavelength region that affects some of the photooxidation processes (Carter et al, 1995b).

This report describes a new state-of-the-art environmental chamber facility developed to minimize reactor effects in studies of VOC reactivity and provide a platform for low NO_x and VOC ozone reactivity and secondary aerosol formation experiments. It also provides the technical background of the facility and assesses its ability and limitations for low NO_x experiments. Results of representative experiments utilizing the chamber, and evaluations of the current SAPRC-99 chemical mechanism using the data obtained, are also presented.

FACILITY DESCRIPTION

The chamber facility comprises a 6m x 6m x 12m thermally insulated enclosure that is continually flushed with purified air at a rate of 1000 L min^{-1} and is located on the second floor of a laboratory building specifically designed to house it. Located directly under the enclosure on the first floor is an array of gas-phase continuous and semi-continuous gas-phase monitors. Within the enclosure are two ~90 m^3 (5.5 m x 3 m x 5.5 m) maximum volume 2 mil FEP Teflon® film reactors, a 200 kW Argon arc lamp, a bank of 115 W 4-ft blacklights, along with the light monitoring and aerosol instrumentation. A schematic of the enclosure is provided in Figure 1.

Enclosure

The interior of the thermally insulated 450 m^3 enclosure is lined with hard clear anodized aluminum sheeting to maximize the interior light intensity and homogenize the interior light intensity. A positive pressure is maintained between the enclosure and the surrounding room to reduce contamination of the reactor enclosure by the surrounding building air. The enclosure air is well mixed by the large air handlers that draw in air from inlets around the light and force the air through a false ceiling with perforated reflective aluminum sheets. The enclosure is temperature controlled with a ~30 ton (~105 KW cooling power) air conditioner capable of producing a temperature range of 5 to 45 C, controlled to better than ±1 C.

Teflon Reactors

The 2 mil (54 μm) FEP Teflon® reactors are mounted within the enclosure with a rigid bottom frame and a moveable top frame. The floor of the reactor is lined with Teflon® film with openings for reactant mixing within and between reactors and 8 ports ranging in size from 0.64 to 1.3 cm for sample injection and withdrawal. The moveable top frame is raised and lowered with a motorized pulley system, which enables the user to expand (during filling) and contract (during an experiment or for flushing) the reactors as necessary. The rate of contraction or expansion is set to maintain a differential pressure of 5 pascal between the inside of the reactor and the enclosure. During experiments, the top frames are slowly lowered to maintain positive pressure as the volume decreases due to sampling, leaks, and permeation. The experiment is terminated when the final reactor volume reaches 1/3 of its maximum value (typically about 10 hours, though less if there are leaks in a reactor). The elevator system coupled with differential pressure measurements allows for repeatable initial chamber volumes and allows for reactants to be injected with greater than 5% precision. The Teflon reactors are built in-house using a PI-G36 Pac Impulse Sealer (San Rafael, CA) heat sealing device for all major seams and are mounted to the reactor floor and ceiling.

The Teflon reactors tend to eventually crack and leak after repeated use, with the failures usually occurring at the seams. Because of the positive pressure control this results in shorter times for experiments rather than dilution or contamination of the reactor. Leaks are repaired using a polyester film tape with a silicone adhesive (3M Polyester Tape 8403) when needed, and the reactors are repaired periodically before leaks and repairs become excessive.

Pure Air System

An Aadco 737 series (Cleves, Ohio) air purification system produces compressed air at rates up to 1500 L min^{-1}. The air is further purified by passing through canisters of Purafil® and heated Carulite
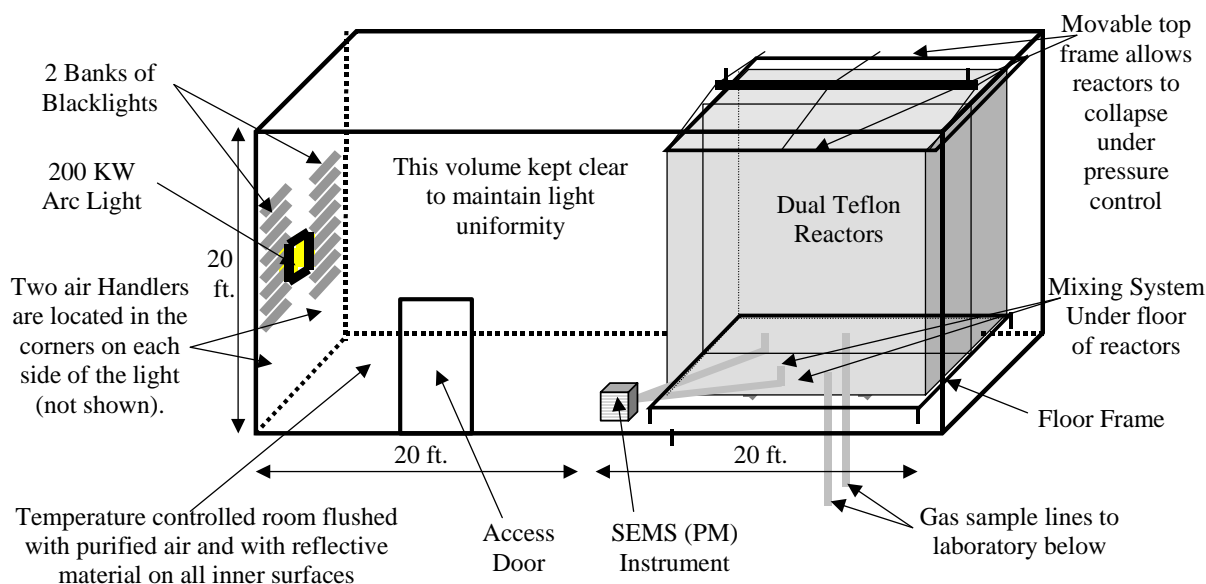
Figure 1.   Schematic of the environmental chamber reactors and enclosure.

300® followed by a filter pack to remove all particulate. The purified air within the reactor has no detectable non-methane hydrocarbons (<1 ppb), NO_x (<10 ppt), no detectable particles (<0.2 particles cm^{-3}), and a dew-point below -40 C.

All the experiments discussed in this report were carried out with unhumidified air, i.e., with a dew point below -40 C. A humidification system has now been constructed, and this system and results of humidified experiments will be discussed in subsequent reports or publications.

The reactors are cleaned between runs by reducing the reactor volume to less than 5% of its original volume and re-filling it to its maximum volume with purified air at least six times. No residual hydrocarbons, NO_x, or particles are detected after the cleaning process.

Light sources

A 200 kW Argon arc lamp with a spectral filter (Vortek co, British Columbia, Canada) is used as the primary means to irradiate the enclosure and closely simulate the entire UV-Visible ground-level solar spectra. The arc lamp is mounted on the far wall from the reactors at a minimum distance of 6m to provide uniform lighting within both reactors. Backup lighting is provided by banks of total 80 1.22 m, 115-W Sylvania 350BL blacklamps (peak intensity at 350 nm) mounted on the same wall of the enclosure. These provide a low-cost and efficient UV irradiation source within the reactor for experiments where the closer spectral match provided by the Argon arc system is not required. The light spectra and intensity characterization for these sources are discussed below.

Interreactor and Intrareactor mixing

The two reactors are connected to each other through a series of custom solenoid valves and blowers. The system provides for rapid air exchange prior to the start of an experiment ensuring, that both

reactors have identical concentrations of starting material. Each reactor can be premixed prior to the start of an experiment by Teflon coated fans located within the reactor.

Instrumentation

Table 1 gives a listing of the analytical and characterization instrumentation whose data were utilized in the experiments discussed in this report. The table includes a brief description of the equipment, species monitored, and their approximate sensitivities, where applicable. These are discussed further below.

Ozone, CO, NO, and NO_y were monitored using commercially available instruments as indicated in Table 1. A second ozone analyzer, based on the chemiluminescence method, was utilized in some experiments, and its data were consistent with the UV absorption instrument listed in Table 1. The instruments were spanned for NO, NO_2, and CO and zeroed prior to most experiments using the gas calibration system indicated in Table 1, and a prepared calibration gas cylinder with known amounts of NO and CO. O_3 and NO_2 spans were conducted by gas phase titration using the calibrator during this period. Span and zero corrections were made to the NO, NO_2, and CO data as appropriate based on the results of these span measurements, and the O_3 spans indicated that the UV absorption instrument was performing within its specifications.

As discussed by Carter (2002), two Tunable Diode Laser Absorption Spectroscopy (TDLAS) are available at our laboratories, with the potential for monitoring up to four different species. TDLAS analysis is described in detail elsewhere (Hastie et al., 1983; Schiff et al., 1994) and is based on measuring single rotational - vibrational lines of the target molecules in the near to mid infrared using laser diodes with very narrow line widths and tunability. The sample for analysis is flushed through closed absorption cells with multi-pass optics held at low pressure (~25 Torr) to minimize spectral broadening. Because of the narrow bandwidth of the diode lasers required to get the highly species-specific measurement, usually separate diode lasers are required for each compound being monitored. Both TDLAS systems have two lasers and detection systems, permitting analysis of up to four different species using this method. However, for most experiments discussed in this report, only one detector was operational for each instrument, one for monitoring NO_2 and the other for monitoring formaldehyde.

The TDLAS NO_2 measurements were calibrated as using the NO_2 span measurements made by gas phase titration with the gas calibrator at the same time the NO-NO_y analyzer was calibrated. Span data were taken in conjunction with most experiments, and these data were used to derive span factors for the entire data set. The TDLAS formaldehyde measurements were calibrated using a formaldehyde permeation source that in turn was calibrated based on Wet chemical calibration procedure using Purpald reagent (Jacobsen and Dickinson, 1974; Quesenberry and Lee, 1996; NIOSH, 1994)

Organic reactants other than formaldehyde were measured by gas chromatography with FID detection as described elsewhere (Carter et al, 1993, 1995b); see also Table 1. The gaseous compounds ethylene, propylene, n-butane and trans-2-butene were monitored by using 30 m megabore GS-Alumina column and the loop sampling system. The second signal of the same GC outfitted with FID, loop sampling system and 30 m megabore DB-5 column was used to analyze surrogate liquid components toluene, n-octane and m-xylene. Low volatility, more "sticky" test compounds were monitored on a second GC-FID using the Tenax cartridge sampling system. The Tenax GC system was calibrated by preparing methanol solutions of the analyzed compound and placing measured amounts of the solution directly on the Tenax® cartridge for subsequent desorption onto the column.

Table 1.   List of analytical and characterization instrumentation used with the chamber.

Type	Model or Description	Species	Sensitivity	Comments
Ozone Analyzer	Dasibi Model 1003-AH. UV absorption analysis. Also, a Monitor Labs Chemiluminescence Ozone Analyzer Model 8410 was used as a backup.	O_3	2 ppb	Standard monitoring instrument.
NO - NO_y Analyzer	Teco Model 42 C with external converter. Chemiluminescent analysis for NO, NOy by catalytic conversion.	NO NO_y	1 ppb 1 ppb	Useful for NO and initial NO_2 monitoring. Converter close-coupled to the reactors so the "NO_y" channel should include HNO_3 as well as NO_2, PANs, organic nitrates, and other species converted to NO by the catalyst.
CO Analyzer	Dasibi Model 48C. Gas correlation IR analysis.	CO	50 ppb	Standard monitoring instrument
TDLAS #1	Purchased from Unisearch Inc. in 1995, but upgraded for this chamber. See Carter (2002). Data transmitted to DAC system using RS-232.	NO_2 HNO_3	0.5 ppb ~ 1 ppb	NO_2 data from this instrument are considered to be interference-free. HNO_3 data are not available for many of the experiments discussed for this report.
TDLAS #2	Purchased from Unisearch Inc. for this chamber. See Carter (2002). Data transmitted to DAC system using RS-232.	HCHO H_2O_2	~ 1 ppb ~2 ppb	Formaldehyde data from this instrument are considered to be interference-free. H_2O_2 data were not taken during most of the experiments discussed in this report
GC-FID #1	HP 5890 Series II GC with dual columns, loop injectors and FID detectors. Controlled by computer interfaced to network.	VOCs	~10 ppbC	30 m x 0.53 mm GS-Alumina column used for the analysis of light hydrocarbons such as ethylene, propylene, n-butane and trans-2-butene and 30 m x 0.53 mm DB-5 column used for the analysis of C_{5+} alkanes and aromatics, such as toluene and m-xylene. Loop injection suitable for low to medium volatility VOCs that are not too "sticky" to pass through valves.
GC-FID #2	HP 5890 Series II GC with dual columns and FID detectors, one with loop sampling and one set up for Tenax cartridge sampling. (Only the Tenax cartridge system used for this project.) Controlled by computer interfaced to network.	VOCs	1 ppbC	Tenax cartridge sampling used for low volatility or moderately "sticky" VOCs that cannot go through GC valves but can go through GC columns. A 30 m x 0.53 mm DB-1701 column was used during most of the period covered by this report.

Table 1 (continued)

Type	Model or Description	Species	Sensitivity	Comments
Luminol GC	Developed and fabricated at CE-CERT based on work of Gaffney et al (1998). Uses GC to separate NO2 from PAN and other compounds and Luminol detection for NO2 or PAN. Data transmitted to the DAC system using RS-232.	NO_2	~0.5 ppb	NO_2 measurements were found to have interferences by O_3 and perhaps other species and were not used for mechanism evaluation.
		PAN	~0.5 ppb	Reliability of measurement for PAN not fully evaluated. Calibration results indicate about a 30% uncertainty in the spans. However, interferences are less likely to be a problem than for NO_2.
Total Hydrocarbon analyzer, FID	Ratfisch Instruments, Model RS 55CA	VOCs	50 ppb	Standard commercial instrument. Used for injection tests only.
Gas Calibrator	Model 146C Thermo Environmental Dynamic Gas Calibrator	N/A	N/A	Used for calibration of NO_x and other analyzers. Instrument acquired early in project and under continuous use.
Data Acquisition Sytem	Windows PC with custom LabView software, 16 analog input, 40 I/O, 16 thermo-couple, and 8 RS-232 channels.	N/A	N/A	Used to collect data from most monitoring instruments and control sampling solenoids. In-house LabView software was developed using software developed by Sonoma Technology for ARB for the Central California Air Quality Study as the starting point.
Temperature sensors	Various thermocouples, radiation shielded thermocouple housing	Tempera-ture	~0.1 ^{o}C	Primary measurement is thermocouples inside reactor. However, comparison with temperature measurements in the sample line suggest that irradiative heating may bias these data high by ~2.5^{o}C. See text.
Humidity Monitor	General Eastern HYGRO-M1 Dew Point Monitor	Humid-ity	Dew point range: -40 - 50°C	Instrument performs as expected, but dew point below the performance range for most of the experiments discussed in this report, except for those with added humidity.
Spectro-radiometer	LiCor LI-1800 Spectroradiometer	300-850 nm Light Spect-rum	Adequate	Resolution relatively low but adequate for this project. Used to obtain relative spectrum. Also gives an absolute intensity measurement on surface useful for assessing relative trends.
QSL Spherical Irradiance Sensor	Biospherical QSL-2100 PAR Irradiance Sensor. Responds to 400-700 nm light.	Spherical Broad-band Light Intensity	Adequate	Provides a measure of absolute intensity and light uniformity that is more directly related to photolysis rates than light intensity on surface. Gives more precise measurement of light intensity trends than NO_2 actinometry, but is relatively sensitive to small changes in position.

Table 1 (continued)

Type	Model or Description	Species	Sensitivity	Comments
Scanning Electrical Mobility Spectrometer (SEMS)	TSI 3080L column, TSI 3077 [85]Kr neutralizer, and TSI 3760A CPC. Instrument design, control, and operation Similar to that described in Cocker et al. (2001)	Aerosol number and size distribut-ions	Adequate	Provides information on size distribution of aerosols in the 28-730 nm size range, which accounts for most of the aerosol mass formed in our experiments. Data can be used to assess effects of VOCs on secondary PM formation.

Both the GC instruments were controlled and their data were analyzed using HPChem software installed on a dedicated PC. The GC's were spanned using the prepared calibration cylinder with known amounts of ethylene, propane, propylene, n-butane, n-hexane, toluene, n-octane and m-xylene in ultrapure nitrogen. Analyses of the span mixture were conducted approximately every day an experiment was run, and the results were tracked for consistency.

As indicated in Table 1, aerosol number and size distributions were also measured in conjunction with many of our experiments. The instrumentation employed is similar to that described by Cocker et al. (2001). Particle size distributions are obtained using a scanning electrical mobility spectrometer (SEMS) (Wang and Flagan, 1990) equipped with a 3077 [85]Kr charger, a 3081L cylindrical long column, and a 3760A condensation particle counter (CPC). Flow rates of 2.5 LPM and 0.25 LPM for sheath and aerosol flow, respectively, are maintained using Labview 6.0-assisted PID control of MKS proportional solenoid control valves. Both the sheath and aerosol flow are obtained from the reactor enclosure. The data inversion algorithm described by Collins et al (2002) converts CPC counts versus time to particle size distribution.

Most of the instruments other than the GCs and aerosol instrument were interfaced to a PC-based computer data acquisition system under the control of a LabView program written for this purpose. The TDLAS instruments were controlled by their own computers, but the data obtained were sent to the LabView data acquisition system during the course of the experiments using RS-232 connections. These data, and the GC data from the HP ChemStation computer, were collected over the CE-CERT computer network and merged into Excel files that are used for applying span, zero, and other corrections, and preparation of the data for modeling.

RESULTS

Light Characterization

Photolysis rates used when modeling chamber experiments are calculated using the measured NO_2 photolysis rates, the relative measured spectral distributions for the light sources, and the absorption cross sections and quantum yields for NO_2 and the other photolysis reactions in the chemical mechanism being evaluated. Therefore the measured NO_2 photolysis rates serve as the measure of the absolute light intensity, and the *relative* spectral distributions of the light sources serve as the means to calculate the other photolysis rates relative to that for NO_2. The precisions of the photolysis rates so derived are determined primarily by the precision of the NO_2 actinometry measurement. These are described below.

Argon arc lamp

All the UCR EPA experiments modeled in this work were carried out using the same Vortek solar simulator power (400 amps), so the light intensity should be essentially constant from run to run if the light is performing up to specifications. The results of the various light intensity measurements made during the course of these experiments were consistent with this expectation. This is shown on Figure 2, which shows plots of various light intensity measurements against EPA run number for the period of the experiments discussed during this report and for subsequent experiments where the same procedures were used. Most of the data concerning the variability in light intensity cam from the QSL PAR radiation meter, which was located in the enclosure about 1 meter in front of the reactors facing the light. These data showed less than 5% variability in total light intensity between run 60 through run ~250. In addition, periodic NO_2 actinometry (k_1) measurements were made with the quartz tube also located in the enclosure about 1 meter in front of the reactors, above the location of the PAR meter, These data also indicated run-to-run variability of less than 5%, and gave an average NO_2 photolysis rate of 0. 0.284 ± 0.010 min^{-1}.

The location of the NO_2 actinometry tube for most of the experiments was outside the reactors and located somewhat closer to the light source than the gases in the reactor, so one would expect the 0.284 min^{-1} average value from those measurements to be somewhat higher than that appropriate for modeling. To obtain measures of absolute light intensity of more direct relevance for modeling, occasional special actinometry experiments were conducted with the quartz actinometry tube located inside one of the reactors. The data obtained, shown on Figure 2, again indicate no trend in NO_2 photolysis rate during this period, and give an average of 0.260 ± 0.004 min^{-1}, with the differences in averages for the two reactors less than 3%. This is about 8% less than the measurement outside the reactor and slightly closer to the light, which is in the expected range.

Since the results of the actinometry measurements shown on Figure 2 indicate no significant changes in light intensity during the period of these experiments, they were all assumed to have the same NO_2 photolysis rate for modeling purposes, which was 0.26 min^{-1}, the average of the in-chamber actinometry results. The other photolysis rates were calculated using this, the assigned spectral distribution (shown on Figure 3) and the absorption cross-sections and quantum yields given with the mechanism.

The relative spectrum of the arc light source was measured using a LI-COR LI-1800 spectroradiometer, and is shown on Figure 3. (The data are normalized to the same NO_2 photolysis rate because that is how they are used to derive photolysis rates in the experiments. The instrument does not measure the spherically integrated absolute intensities needed to directly calculate photolysis rates, but its
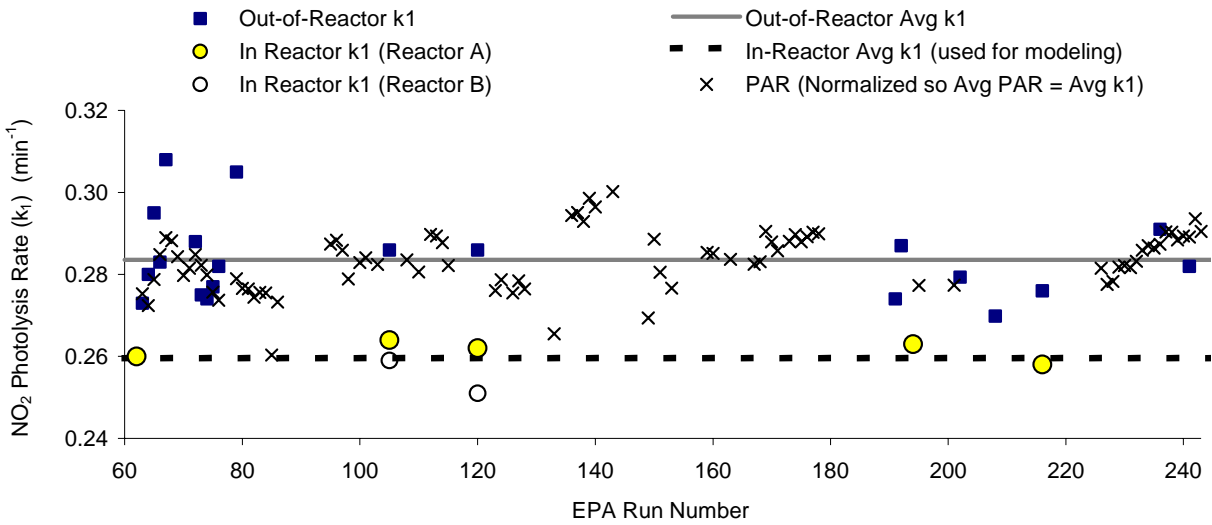
Figure 2.   Plots of various measures of light intensity for the EPA chamber experiments against EPA run number.
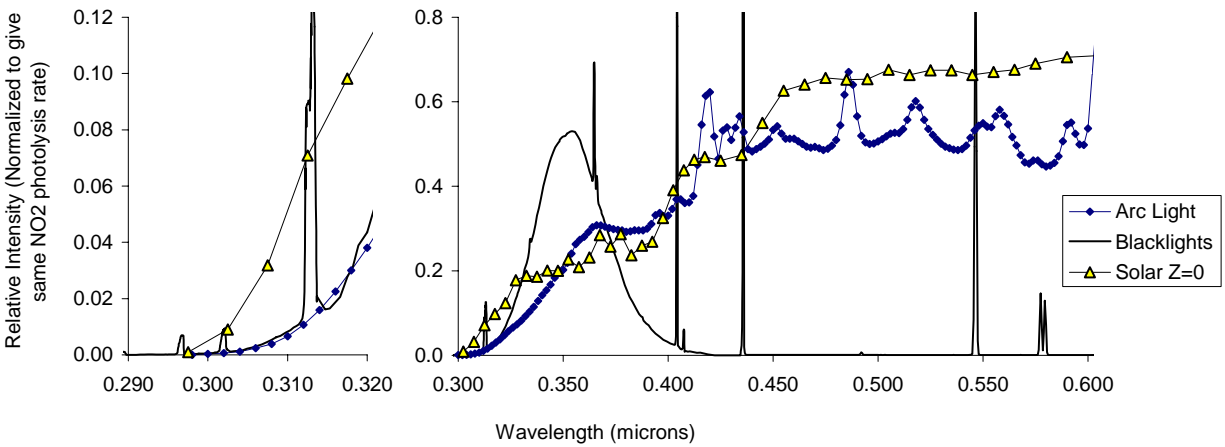

Figure 3.   Spectrum of the light sources used in the chamber, with relative intensities normalized to give the same NO_2 photolysis rate. A representative solar spectrum is shown for comparison.

data are useful for relative measurements.) No appreciable change in the light source spectrum was observed since this light source has been in operation.

Blacklamps

Blacklights tend to decrease in intensity in time as they are used (Carter et al, 1995b), and this needs to be taken into account when assigning photolysis rates when modeling blacklight experiments. Relevant information concerning the intensity of this light source comes from the following sources:

- A few NO_2 actinometry measurements were made using the quartz tube method of Zafonte et al (1977), modified as discussed by Carter et al (1995b) with the quartz tube inside the reactors. These were used as the standard to derive absolute photolysis rates within the chamber, but were insufficient in number to verify trends in light intensity with time.

- NO_2 actinometry measurements were also made with the quartz tube located in the "standard" position in front of the reactors and between the reactors and the light source. Since the tube is closer to the light than the reactors, these measurements are expected to be higher than the in-chamber photolysis rates. Figure 5a shows plots of in-reactor NO2 photolysis rates against measurements in the standard location made on the same day. The data are fit by a line through zero with a slope of 0.698, which is also shown on Figure 4a. This correction factor was used to derive in-chamber NO_2 photolysis rates from measurements in the standard position.

- The most useful dataset for determining how light intensity varied with time came from the QSL Spherical irradiance sensor located in front of the reactors near the NO_2 actinometry tube in the "standard" location. Data from this sensor are available for almost all experiments, and averages during the experiments are used as the relative measure of light intensity during the run. These data are calibrated by comparing results of in-chamber NO_2 actinometry measurements and standard QSL measurements appropriate for the time of the actinometry measurements (derived as discussed below), and the results are shown on Figure 4b. The line shows the least squares line fit through the data, which can be used to derive in-chamber NO_2 photolysis rates from averages of the QSL measurements made during the experiments.

Since blacklight experiments were conducted only intermittently and the blacklights were not used during the arc light experiments, the EPA run number did not provide a useful measurement of the aging of the light source for estimating the trends in light intensity with time. Instead, the "blacklight run count", which is the number of experiments carried out using blacklights up to the time of the experiment being considered, is used for this purpose. Plots against blacklight run count of in-chamber NO_2 photolysis rates derived by direct measurement or from the actinometry measurements in the "standard" location or from the QSL data from the fits shown on Figure 4a and Figure 4b are shown on Figure 4c. It can be seen that up to blacklight run count 110 (around run EPA384) the actinometry results and most of the QSL data are well fit by a straight line, which can be used as a basis for assigning NO_2 photolysis rates for individual experiments. After around the time of EPA384 the QSL data indicate that the light intensity no longer declines significantly.

Figure 4 shows that not all the QSL measurements were well fit by the trend line. In general, the outliers tended to be QSL measurements from experiments where the QSL was not in the standard location, or where there were indications that QSL measurements were being affected by structures within the enclosure. These data were not used in determining the trend line. Note that a similar trend line was used to derive the QSL values for the times of the in-chamber NO_2 actinometry measurements for the purpose of relating the QSL data to the in-chamber NO_2 photolysis rates as shown on Figure 4b. This permitted the use of the QSL data to derive the trend line shown on Figure 4c used for estimating NO_2 photolysis rates for individual experiments.
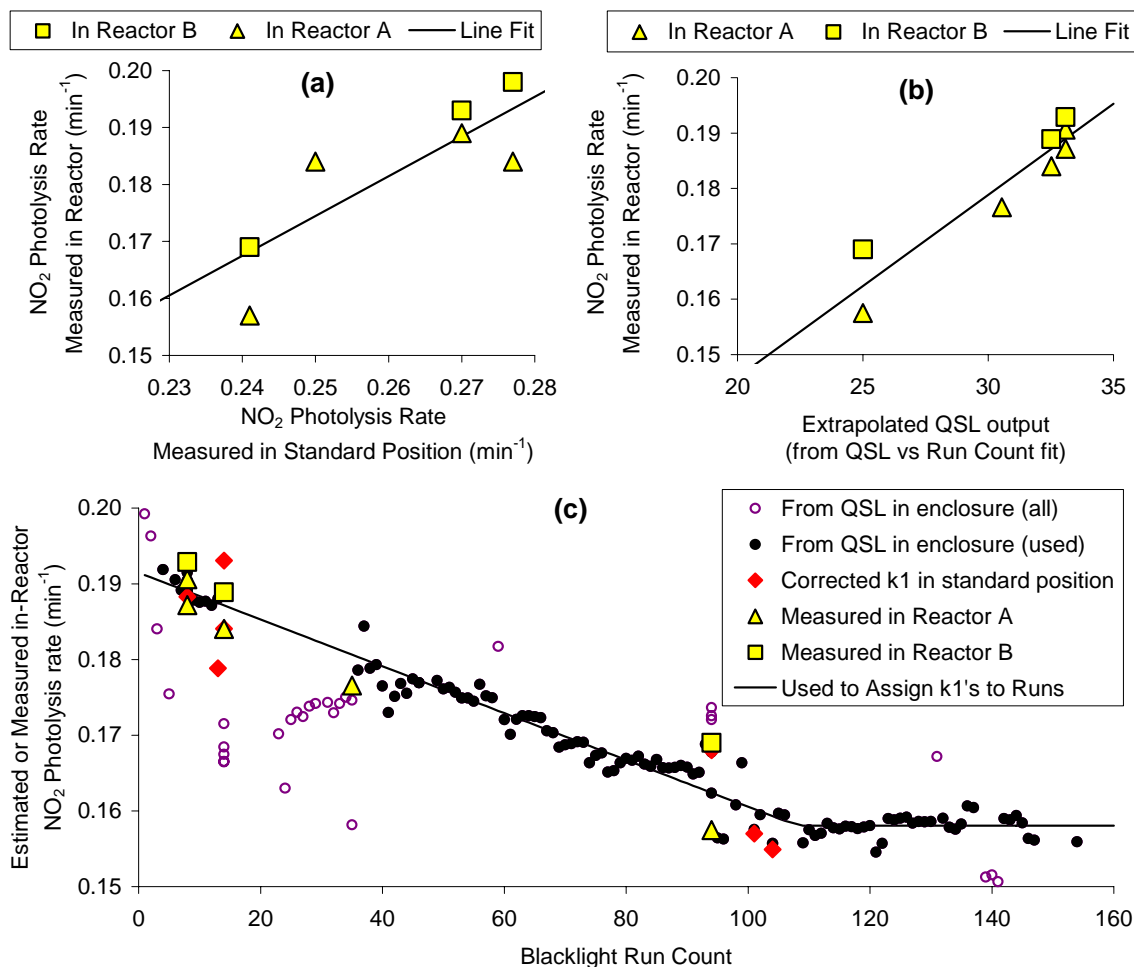
Figure 4.   Plots of light intensity data used to assign NO_2 photolysis rates for the blacklight light source.

The results of this analysis indicates that the NO_2 photolysis rate for blacklight experiments declines from about 0.191 min^{-1} when the lights were first installed to about 0.158 at the time of blacklight run count 110 (EPA384), and then levels off at that value. This was used when deriving photolysis rates for experiments using this light source. The reason why the decline in intensity apparently ends around the time of run EPA384 is unknown.

The spectrum of this light source was measured using the LiCor 1800 spectroradiometer and was found to be essentially the same as that recommended by Carter et al (1995a) for modeling blacklight chamber runs, and did not change with time. This spectrum is shown on Figure 2.

Temperature Characterization

The temperature in each of the reactors was continuously measured using thermocouples located inside the reactor and also, for many experiments, using thermocouples located inside the sample line. It was found that the temperatures in the two reactors were essentially the same when their thermocouples

16

were in comparable locations, but temperatures measured in the sample line were only the same as those in the reactors when the arc light was off. The temperatures monitored in both locations increased when the light was turned on, but the temperature measurement in the sample line rose much more slowly and stabilized at a lower level. An example of this is shown on Figure 5, which shows the measured temperature data for run EPA-123. This could be due to temperature inertia in the sample line, which takes a period of time to heat after the lights are turned on. However, the difference was consistent after about 4 hours of irradiation, with the average difference being 2.5°C. Based on this, we conclude that temperature measured inside the reactor probably gives the better measure of how the temperatures changes with time, but that once it is stabilized the temperature in the sampling line is likely to have less bias because it is not exposed to the direct light.

Based on this, for modeling purposes we assume that the temperature inside the reactor is reflected by the readings of the thermocouples inside the reactor, corrected by subtracting 2.5°C. Since the temperature appears to be relatively stable after about 1-2 hours for modeling in this work we represent the temperature as being constant at the average value. Although strictly speaking it would be better to represent the ~3°C rise in temperature during the first 1-2 hours in the model input, test calculations showed that using the more exact representation of the temperature variation had essentially no effect on predictions of O_3 and other species used in this evaluation. Figure 5 shows the average temperature used for modeling the example experiment shown there.

Characterization of Contamination by Outside Air

Minimizing contamination of the reactor by leaks and permeation of laboratory air contaminants was an important design goal of the new reactors. This is accomplished by providing clean air within the enclosure that houses the reactors. Continuous monitoring of the enclosure contents demonstrates that NO_x and formaldehyde levels in the enclosure before or during irradiations are less than 5 ppb and PM concentrations are below the detection limits of our instrumentation (see Table 1). Introduction of contaminants into the reactor is also minimized by use of pressure control to assure that the reactors are always held at slight positive pressures with respect to the enclosure. Thus leaks are manifested by reduction of the reactor volume rather than dilution of the reactor by enclosure air. The leak rate into the chamber was tested by injecting ~100 ppm of CO into the enclosure and monitoring CO within the reactor for more than 6 hours. In addition, since CO is a small molecule, it should provide an upper limit of leak plus permeation into the reactor. No appreciable CO (above the 50 ppb detection limit) was
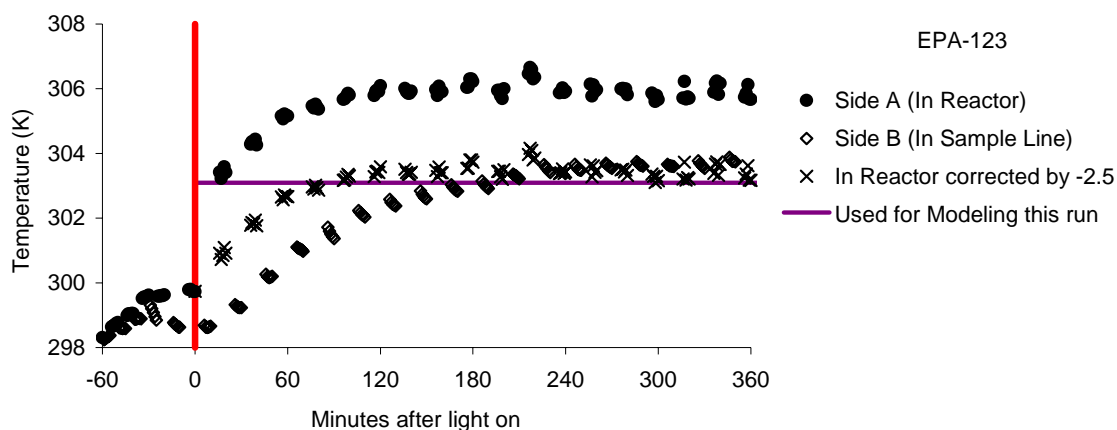

Figure 5.   Plot of temperature measurements made during run EPA123.

17

obtained for this experiment. Therefore it was concluded that leaks/permeation into the chamber is negligible for the current reactor configuration.

Chamber Effects Characterization

It is critical to understand the impact of reactor walls on gas-phase reactivity and secondary aerosol formation. Larger volume reactors may minimize these effects, but they cannot be eliminated entirely or made negligible. For mechanism evaluation and SOA studies the most important of these effects include background offgasing of NO_x and other reactive species, offgasing or heterogeneous reactions that cause "chamber radical sources" upon irradiation (e.g., see Carter et al, 1982), ozone and particle losses to the reactor walls, and background offgasing of PM or PM precursors. Most of these can be assessed by conducting various types of characterization experiments that either directly measure the parameter of interest, or are highly sensitive to the chamber effect being assessed (e.g., see Carter et al, 1995a). The chamber effects relevant to gas-phase mechanism evaluation that have been assessed and the types of experiments utilized for assessing them are summarized in Table 2. These are discussed further below.

Note that as indicated in Table 2 some of the chamber characterization parameters are derived by conducting model simulations of the appropriate characterization experiments to determine which parameter values best fit the data. All the characterization simulations discussed here were carried out using the SAPRC-99 chemical mechanism (Carter, 2000) with the photolysis rates calculated using the light characterization data discussed above, using the measured temperatures of the experiments, and assuming no dilution for reasons discussed in the previous section. The rates of heterogeneous reactions not discussed below, such as N_2O_5 hydrolysis to HNO_3 or NO_2 hydrolysis to HONO, were derived or estimated based on laboratory studies or other considerations as discussed by Carter et al (1995a). Although the assumed values of these parameters can affect model simulations under some conditions, they are not considered to be of primary importance in affecting simulations of the characterization or other experiments discussed here.

NO_x offgasing

NO_x offgasing is the main factor limiting the utility of the chamber for conducting experiments under low NO_x conditions. Although this can be derived by directly measuring increases in NO_x species during experiments when NO_x is not injected, the most sensitive measure is the formation of O_3 in irradiations when VOCs but not NO_x are initially present. Therefore, the NO_x offgasing rate is not determine directly, but derived by determining the magnitude of the NO_x offgasing rates that it is necessary to assume in the chamber effects model for the model simulations of the experiments to correctly predict the experimentally observed O_3 yields. The NO_x offgasing can be represented in the model as inputs of any species that rapidly forms NO_x in atmospheric irradiation systems, such as NO, NO_2, or HONO (which rapidly photolyzes to form NO, along with OH radicals), but for reasons discussed below it is represented in our chamber effects model as offgasing of HONO, e.g.,

$$\text{Walls} + h\nu \rightarrow \text{HONO} \qquad \qquad \text{Rate} = k_1 \text{ x RN}$$

Where k_1 is the light intensity as measured by the NO_2 photolysis rate, and RN is the NO_x (and radical) offgasing parameter, which is derived by model simulations of the appropriate characterization experiments to determine which value best fits the data.

The NO_x offgasing rates necessary to use in the model simulations to predict the observed O_3 formation rates in the CO - air, formaldehyde - air and CO - formaldehyde - air experiments carried out in the first eight months of operation of this chamber are shown as the triangle symbols in Figure 6. The

Table 2.   Summary of types of characterization experiments and types of chamber effects parameters relevant to gas-phase mechanism evaluation derived from these experiments.

Run Type	No. Runs	Sensitive Parameters	Comments
Ozone Dark Decay	4	O_3 wall loss rate	The loss of O_3 in the dark is attributed entirely to a unimolecular wall loss process.
CO - Air	8	NO_x offgasing	Insensitive to radical source parameters but O_3 formation is very sensitive to NO_x offgasing rates. Formaldehyde data can also be used to derive formaldehyde offgasing rates.
CO - HCHO - air	2	NO_x offgasing.	Insensitive to radical source parameters but O_3 formation is very sensitive to NO_x offgasing rates. Also can be used to obtain formaldehyde photolysis rates
CO - NO_x	6	Initial HONO, Radical source	O_3 formation and NO oxidation rates are very sensitive to radical source but not sensitive to NO_x offgasing parameters. Formaldehyde data can also be used to derive formaldehyde offgasing rates.
n-Butane - NO_x	1	Initial HONO, Radical source	O_3 formation and NO oxidation rates are very sensitive to radical source but not sensitive to NO_x offgasing parameters.
Pure Air	6+	NO_x offgasing, Background VOCs	Used primarily to screen for background VOC effects with the NO_x offgasing and chamber radical source parameter set at values that fit the other types of characterization experiments.

plots are against the EPA chamber experimental run number, which indicates the order that the experiment was carried out. It can be seen that the rates of around 1.5 ppt/min generally fit the data up to around run 85, then these increased to 2-7 ppt/min after that, being somewhat higher in the "A" reactor compared to the "B" reactor. The reason for this increase is unclear, but it may be related to the fact that maintenance was done to the reactors around the time of the change. The magnitudes of these apparent NO_x offgasing rates are discussed further below in conjunction with the discussion of the continuous radical source, which is also attributed to HONO offgasing.

Chamber radical source

It has been known for some time that environmental chamber experiments could not be modeled consistently unless some sources of radicals attributed to chamber effects is assumed (e.g., Carter et al, 1982; Carter and Lurmann, 1991; Carter, 2000). The most sensitive experiments to this effect are NO_x -air irradiations of compounds, such as CO or alkanes, which are not radical initiators or do not form radical initiating products to a sufficient extent to significantly affect their photooxidations. If no chamber dependent radical source is assumed, model simulations of those experiments predict only very slow NO oxidation and essentially no O_3 formation, while in fact the observed NO oxidation and O_3 formation rates
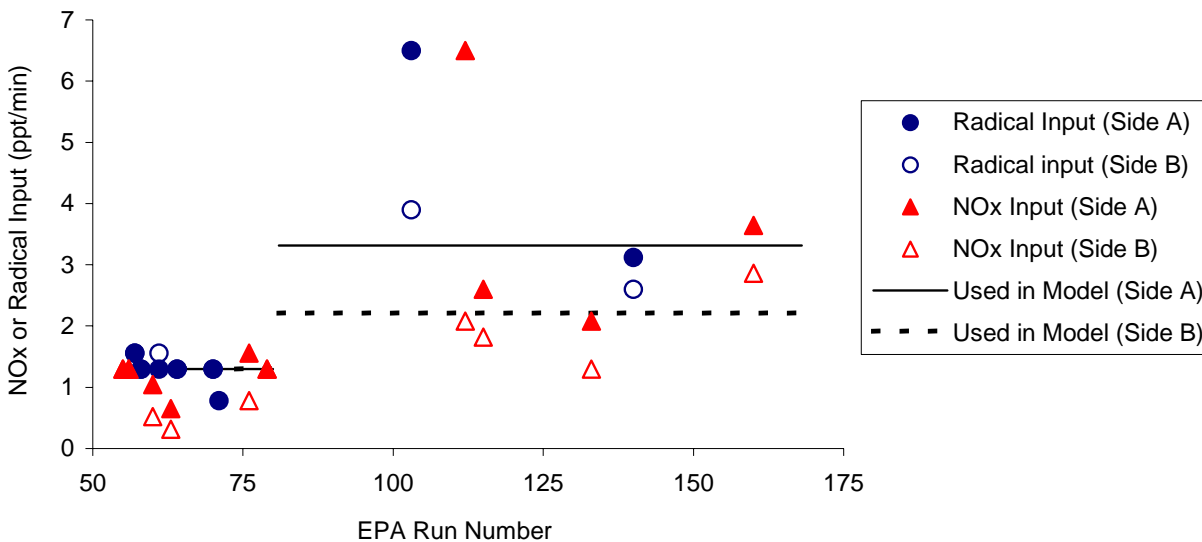
Figure 6.　　Plots of NO_x or radical input rates necessary for model simulations to predict the experimental data against experimental run number (i.e., against the order the experiment was carried out).

are much higher (Carter et al, 1982). It is necessary to assume unknown or chamber-dependent radical sources for the model to appropriately simulate the results of these experiments.

In some chambers at least part of the chamber-dependent radical source can be attributed to formaldehyde offgasing (Simonaitis et al, 1997, Carter, 2004), but as discussed below the magnitude of the formaldehyde offgasing in this chamber is relatively small, and not sufficient by itself for the model to simulate radical-source dependent experiments. For this chamber, assuming HONO offgasing at a similar magnitude as the apparent NO_x offgasing rate derived as discussed above is usually sufficient to account for most of the chamber-dependent radical source, though results of some of the experiments are somewhat better simulated if a small amount (100 ppt or less) of HONO is also assumed to be initially present.

The round symbols in Figure 6 shows plots of the HONO offgasing rates that are necessary to assume in the model simulations for the model to simulate the NO oxidation and O_3 formation rates in the radical-source sensitive CO - NO_x and n-butane - NO_x experiments that were carried out in January-October of 2003. Note that since these experiments had initial NO_x levels ranging from 10 - 200 ppb, so they were not sensitive to NO_x offgasing as such. However, from Figure 6 it can be seen that the magnitudes of the NO_x offgasing and continuous radical input rates that fit the data for the respective characterization experiments were in the same range, and even changed at the same time when the characteristics of the chamber apparently changed. Whatever effect or contamination caused the apparent NO_x offgasing to increase around the time of run 85 caused the same increase in the apparent radical source.

Comparison of Radical Source and NO_x Offgasing with Other Chambers

Although HONO is not measured directly in our experiments, the fact that both the radical-sensitive and NO_x-sensitive characterization experiments can be simulated assuming HONO offgasing at

20

approximately the same rates is highly suggestive that this is the process responsible for both effects. Direct evidence for this comes from the data of Rohrer et al (2004), who used sensitive long path absorption photometer (LOPAP) instrument to detect ppt levels of HONO emitted from the walls during irradiations in the large outdoor SAPHIR chamber (Brauers et al, 2003) at rates comparable to those observed in the earlier experiments in our chamber. The SAPHIR chamber is similar in design to our chamber, except it is larger in volume and is located outdoors. In particular, like our chamber it has Teflon walls and uses an enclosure configuration to minimize contamination by outside air. Therefore, it would be expected to have similar chamber NO_x and radical sources, and this appears to be the case.

Figure 7 shows plots of the NO_x offgasing or radical source parameter (e.g. RN in Equation 1) obtained in modeling appropriate characterization runs in various chambers, where they are compared with direct measurements made in the SAPHIR chamber (Rohrer et al, 2004). In addition to those for this UCR EPA, the radical source parameters shown are those derived by Carter (2000) for previous indoor and outdoor chambers at UCR (Carter et al, 1995a), those derived by Carter and Lurmann (1991) for the University of North Carolina (UNC) outdoor chamber (Jeffries et al, 1982, 1995a-c, 1990), and those derived by Carter (2004) for the Tennessee Valley Authority (TVA) indoor chamber (Simonaitis and Bailey, 1995; Bailey et al, 1996). (Note that the data shown for the UCR EPA chamber includes experiments carried out subsequently to those shown in Figure 6, including a few runs at reduced temperature.) The figure shows that the radical source and NO_x offgasing rates derived for this chamber are comparable in magnitude to the HONO offgasing directly measured in the SAPHIR chamber and also comparable to the NO_x offgasing derived for TVA chamber but are significantly lower than those derived from modeling characterization data from the earlier UCR and UNC chambers. It is interesting to note
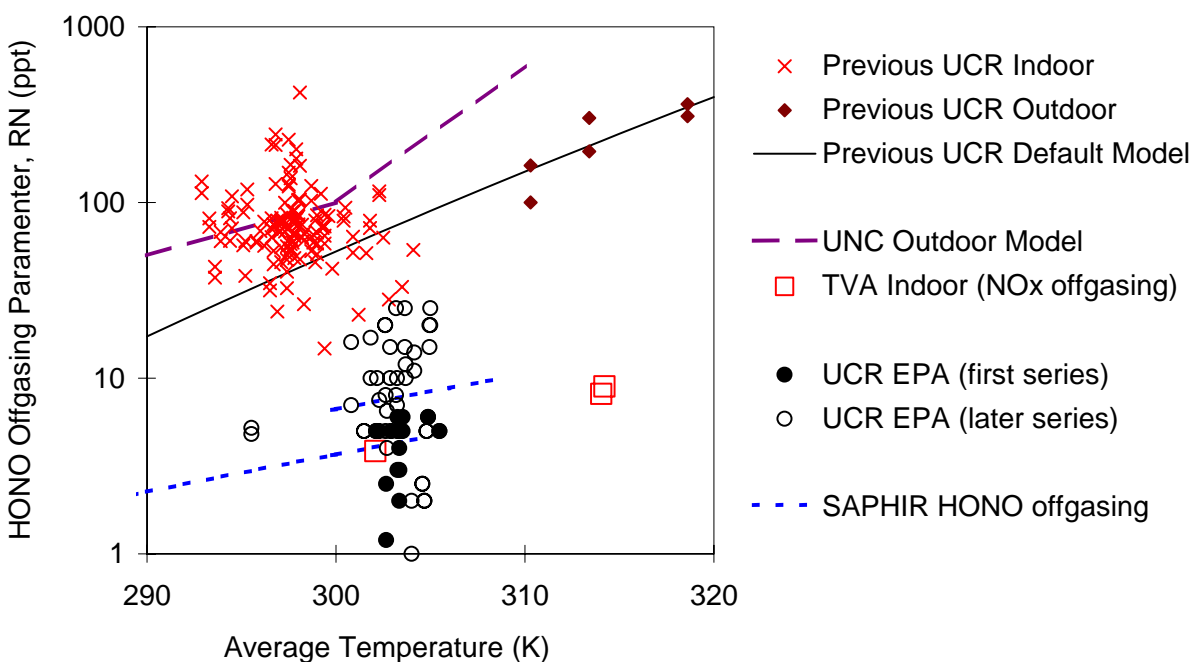

Figure 7.   Plots of the HONO offgasing parameter, RN (ratios of the HONO offgasing rates the NO_2 photolysis rates) derived from modeling characterization runs for various chambers. Data shown are for unhumidified experiments except for the UNC outdoor and TVA chambers.

21

that parameters derived for the various chambers indicate that the radical source and HONO or NO_x offgasing rates all increase with temperature.

Therefore, the radical source and NO_x offgasing rates indicated by the characterization data for the first series of experiments for this chamber is probably as low as one can obtain for reactors constructed of FEP Teflon film, which is generally believed to be the most inert material that is practical for use as chamber walls. Although the radical source and NO_x offgasing rates for the second series of experiments is higher (see also Figure 6), they are still about an order of magnitude lower than observed for the UCR and UNC chambers previously used for mechanism evaluation.

Formaldehyde offgasing

Low but measurable amounts of formaldehyde were formed in irradiations in this chamber, even in pure air, CO - NO_x, or other experiments where no formaldehyde or formaldehyde precursors were injected, and where formaldehyde formation from the reactions of methane in the background air is predicted to be negligible. The data in essentially all such experiments could be modeled assuming a continuous light-dependent formaldehyde offgasing rate corresponding to 0.3 ppb/hour at the light intensity of these experiments. Formaldehyde levels resulting from this relatively low offgasing rate could not be detected with formaldehyde analyzers used in most previous UCR and other chamber experiments, and are insufficient to account for the apparent chamber radical source observed in most chamber experiments. This apparent formaldehyde offgasing has a non-negligible effect on very low VOC and radical source characterization experiments, so it must be included in the chamber characterization model. However, it has a relatively minor impact on modeling most experiments used for VOC mechanism evaluation or reactivity assessment.

The source of the apparent formaldehyde offgasing in the Teflon reactors is unknown, but it is unlikely to be due to buildup of contaminants from previous exposures or contamination from the enclosure. The apparent formaldehyde offgasing rate is quite consistent in most cases and there are no measurable differences between the two reactors. This is despite the fact that the East or "Side B" reactor was constructed several months after the West or "Side A" reactor, which was used in at least 17 experiments before the second reactor was built. In addition the background formaldehyde level in the enclosure was quite variable during this period, and no apparent correlation between this and the apparent formaldehyde offgasing rates in the reactor was observed. The data are best modeled by assuming only direct formaldehyde offgasing, as opposed to some formaldehyde being formed from light-induced reactions of some undetected contaminant.

Other Reactive VOC Background or Offgasing

Because of limitations in the detection and sensitivity of the organic monitoring methods currently available with our chamber, characterization experiments that are sensitive to background reactive VOCs provide the most useful means to assess whether background levels or offgasing of other reactive VOCs are significant. Ozone formation in pure air runs is very sensitive to background reactive VOCs, though it is also sensitive to the NO_x offgasing effects discussed above. The average 6-hour ozone levels in the pure air runs carried out with the arc lights during this period with the chamber in the standard configuration was only 4±2 ppb. This can be compared with the model simulations of the same experiments, using the NO_x and formaldehyde offgasing parameters derived from the other characterization experiments as discussed above, and assuming no other reactive VOCs are present, which gave an average 6-hour O_3 of 6±2 ppb. This indicates that background or offgasing of other reactive VOCs is not significantly affecting results of these experiments, and should have even smaller effects on mechanism evaluation experiments with added reactive VOCs.

Particle wall losses

Particle wall losses are expected in finite volume reactors and are somewhat enhanced by the charged surfaces of the Teflon media. Particle wall losses within chambers have been described in detail in Cocker et al. (2001a). Briefly, wall losses are expected to be described by a first order wall loss mechanism with a weak size dependence for the aerosol sizes typical of SOA experiments. Particle wall loss rates can be determined in any experiment where particles are present for a sufficiently long time that new particle formation is no longer determining. If it is assumed that no new particle formation is occurring, then the decay rate in the particle number can be assumed to be the particle loss rate.

Figure 8 shows plots of particle wall loss obtained from data from various experiments in this chamber from the time particle measurements were made through the summer of 2004. It can be seen that although there is run-to-run variability, the decay rates are reasonably consistent at approximately 7 day^{-1}, with no significant differences among reactors. This is within the range reported for other large chamber facilities (Barnes and Sidebottom, 2000, Griffin, 1999). While the maximum particle volume in the experiments ranged from less than 0.1 to almost 80 μg/m^3, there was no correlation between maximum particle volume and measured decay rate.

Background Particle Formation

The reactor walls could be a source of particles as well as gas-phase species. This could be due to either direct release of particles from the walls during the irradiations, or offgasing of compounds that react to form secondary PM. Background PM formation could also occur if there were impurities in the air that reacted to form secondary PM. This would be manifested by the formation of particles in pure air irradiations or irradiations of reactants that are not expected to form condensable products.

Maximum PM number and PM volume levels measured after 5 hours of irradiation in pure air, CO - air, CO - NO_x - air, and propene - NO_x experiments carried out in the second set of reactors, installed immediately before run 169, are shown on Figure 9. (Characterization data for the first set of
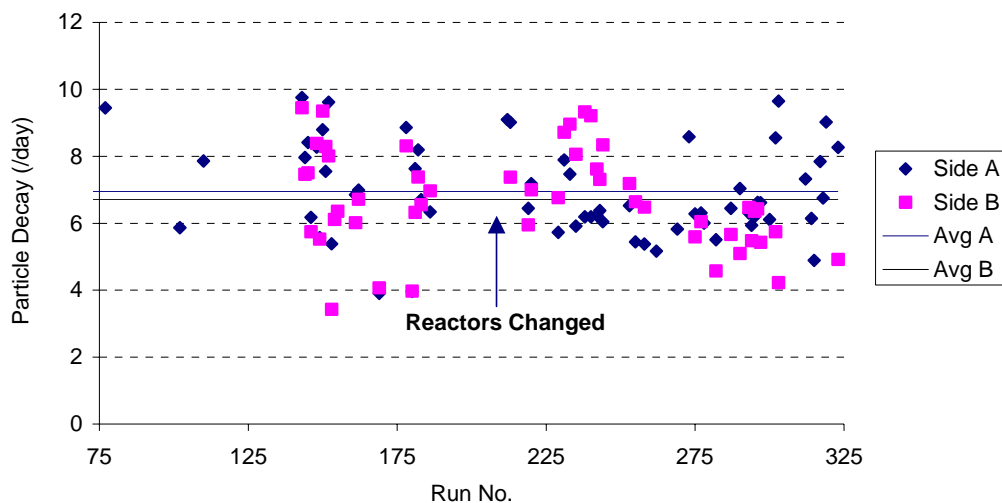

Figure 8.   Plots of particle loss rates against time for experiments from February 2003 through June of 2004.
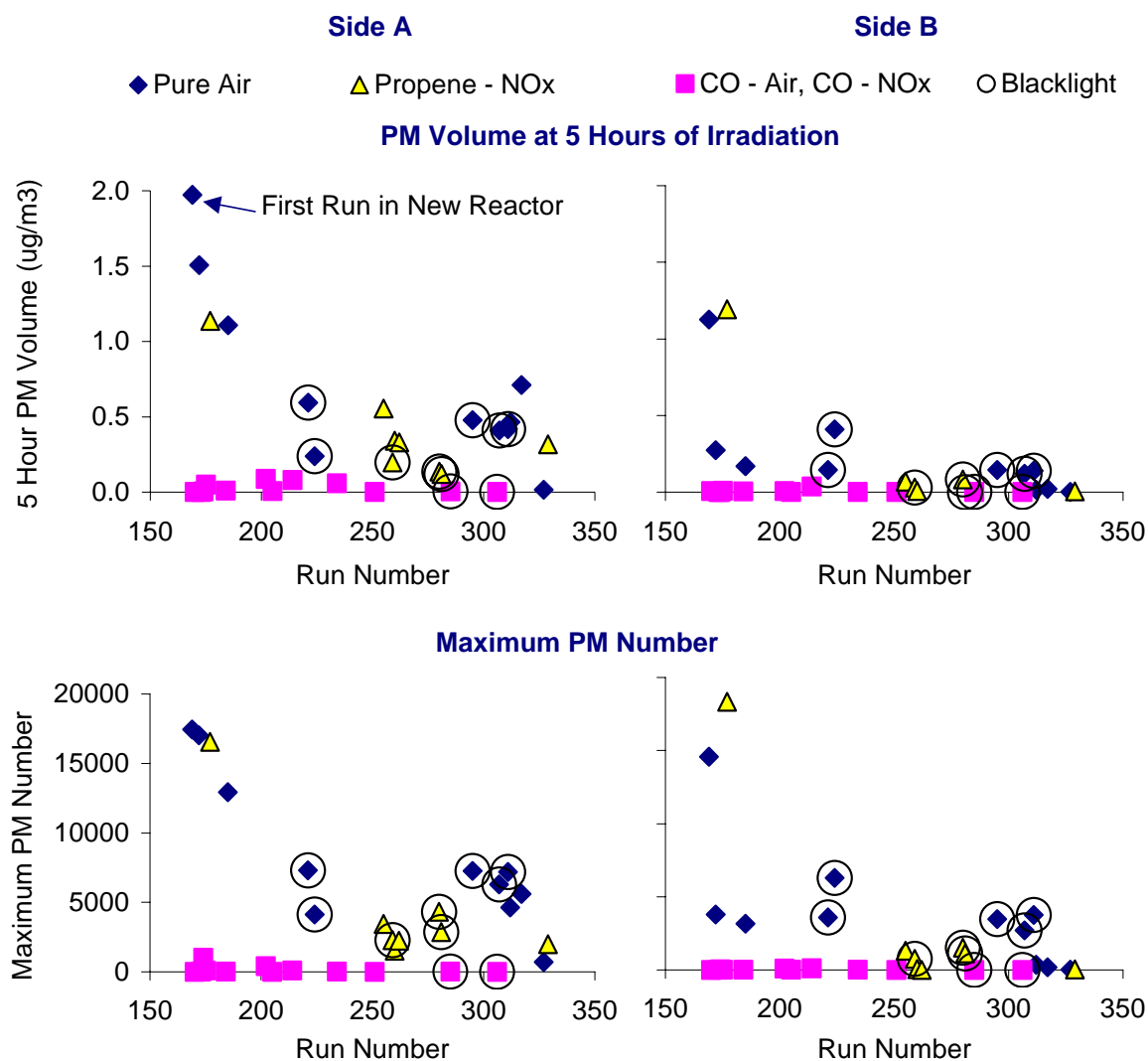
Figure 9.   Plots of 5-Hour PM volume and maximum PM number data in PM background characterization experiments in the reactors installed before run 169.

reactors are sparse but generally consistent with the results shown here.) Measurable PM formation is seen in pure air and propene - NO_x experiments, but essentially no PM formation is seen in the CO - air or CO - NO_x irradiations. The lack of measurable PM in the CO - air or CO - NO_x experiments suggests that PM is not directly emitted from the irradiated walls, though this is considered to be unlikely in the first place. The fact that background PM is formed in the pure air and propene - NO_x experiments but not the CO - air or CO - NO_x experiments could be attributed to PM formation from the reaction of OH radicals with some background contaminant(s). Model calculations predict that OH levels are suppressed in the CO experiments because of its reaction with CO combined with the lack of homogeneous radical sources in CO - air or CO - NO_x systems.

The background PM in the pure air and propene - NO_x experiments is the highest when the rectors were new, and eventually decline as the reactor is used. This suggests that, at least for these

reactors, contaminants due to the experiments are less important than contaminants on the new Teflon film or that are introduced during its construction. The apparent background PM in eventually declined in both reactors, becoming very low in Reactor B, but continued to be non-negligible in Reactor A. Reactor A also had higher levels of background PM at the start.

Although the reaction of O_3 with background contaminants could be another source of background PM, this does not appear to be as significant in this chamber. Higher levels of O_3 are formed in CO - air than in pure air runs, yet the PM levels are much lower in the presence of CO. PM levels in O_3 dark decay experiments are relatively low. In particular, the PM volume in the 0.2 ppm O_3 dark decay experiment 179 was only ~0.1 µg/m^3 in both reactors after ~5 hours, despite the fact that this was during period with new reactors when the background was relatively high. The PM levels increased only slightly when O_3 was irradiated.

Gas-Phase Characterization and Mechanism Evaluation Results

Table 3 gives a summary of the initial experiments carried out in this chamber for gas-phase characterization and mechanism evaluation. All these experiments were carried with unhumidified air (dew point < -40 C), at atmospheric pressure (~740 torr local pressure) and at 303±1 K for arc light runs and at 301±1 K for blacklight experiments. The various characterization experiments were used to derive the chamber characterization parameters and evaluate the chamber characterization model as discussed above. The single organic - NO_x experiments were carried out to demonstrate the utility of the chamber to test the mechanisms for these compounds, for which data are available in other chambers, and to obtain well-characterized mechanism evaluation data at lower NO_x levels than previously available. The formaldehyde + CO - NO_x experiments were carried out because they provided the most chemically simple system that model calculations indicated was insensitive to chamber effects, to provide a test for both the basic mechanism and the light characterization assignments. The aromatic + CO - NO_x experiments were carried out because aromatic - NO_x experiments were predicted to be very sensitive to the addition of CO, because it enhances the effects of radicals formed in the aromatic system on ozone formation. The ambient surrogate - NO_x experiments were carried out to test the ability of the mechanism to simulate ozone formation under simulated ambient conditions at various reactive organic gas (ROG) and NO_x levels.

The ROG surrogate used in the ambient surrogate - NO_x experiments consisted of a simplified mixture designed to represent the major classes of hydrocarbons and aldehydes measured in ambient urban atmospheres, with one compound used to represent each model species used in condensed lumped-molecule mechanism. The eight representative compounds used were n-butane, n-octane, ethene, propene, trans-2-butene, toluene, m-xylene, and formaldehyde. (See Carter et al, 1995c, for a discussion of the derivation of this surrogate).

The ability of the SAPRC-99 mechanism (Carter, 2000) to simulate the total amount of NO oxidized and O_3 formed in the experiments, measured by $([O_3]_{final}-[NO]_{final}) - ([O_3]_{initial}-[NO]_{initial})$, or $\Delta([O_3]-[NO])$, is summarized for the various types of experiments on Table 3 and shown for the individual runs on Figure 10. This gives an indication of the biases and run-to-run variability of the mechanism in simulating ozone formation. In experiments with excess NO the processes responsible for O_3 formation are manifested by consumption of NO, so simulations of $\Delta([O_3]-[NO])$ provides a test of model simulations of these processes even for experiments where O_3 is not formed.

Note that the characterization runs were modeled using the same set of characterization parameters as used when modeling the mechanism evaluation runs, which are based on averages of best fit values for the individual experiments, and not with the values that were adjusted to fit the individual

25

Table 3.   Summary of initial experiments carried out in the chamber.

Run Type [a]	Runs [b]	NOx (ppb)	CO (ppm)	VOC (ppb except as noted)	Average $\Delta(O_3-NO)$ Model Fits [c] Bias	Error
Pure Air	6	0	0	0	See note [d]	
Other Characterization	32	0-202	0-168	0-490	-3%	28%
HCHO – NOx	2	8 - 23		35-50	-23%	23%
HCHO - CO - NOx	2	16 - 21	14-76	39-49	-10%	10%
Ethene – NOx	2	10 - 25		617-650	-15%	15%
Propene – NOx	2	5 - 24		42-52	16%	16%
Toluene – NOx	3	5 - 24		61-152	11%	11%
m-Xylene - NOx (arc light)	1	5		18	6%	6%
m-Xylene - NOx (blacklight)	18	17-100		25-215	[e]	
Toluene - CO - NOx	5	4 - 27	24-50	55-165	-16%	17%
m-Xylene – CO - NOx	1	6 - 6	47	18	-21%	21%
Surrogate - NOx	61 [f]	2 - 315		0.2 - 4.2 [g]	-10%	13%

[a] Arc light used unless indicated otherwise

[b] Each reactor irradiation is counted as a separate run, so two runs are done at once.

[c] Error and bias for model predictions of $\Delta([O_3]-[NO])$ using the SAPRC-99 mechanism. Bias is (calculated - experimental) / calculated. Error is the absolute value of the bias.

[d] The average 6-hour O_3 yields for the pure air runs with blacklights and standard conditions are 4 ± 2 ppb experimental and 6 ± 2 ppb calculated.

[e] Not used for gas-phase mechanism evaluation. See discussion of SOA yield experiments.

[f] Includes experiments carried out for subsequent projects

[g] ppmC

runs. Therefore, the relatively large variability and average model error for the model simulations of $\Delta([O_3]-[NO])$ in those experiments provides a measure of the variability of the chamber effects parameters (e.g., HONO offgasing) to which these experiments are sensitive. The relatively low average bias is expected because the chamber effects parameter values were derived based on these data.

For the single VOC - NO_x or VOC - CO - NO_x experiments, the model is able to simulate the $\Delta([O_3]-[NO])$ to within $\pm25\%$ or better in most cases, which is better than the $\pm\sim30\%$ seen in previous mechanism evaluations with the older chamber data (Carter and Lurmann, 1990, 1991; Gery et al, 1989, Carter, 2000). However, there are indications of non-negligible biases in model simulations of certain classes of experiments. The cleaner conditions and the relatively lower magnitude of the chamber effects may make the run-to-run scatter in the model performance less than in the simulations of the previous data, and this tends to make smaller biases in the model performance more evident. For example, Figure 10 shows that the mechanism tends to underpredict O_3 formation in aromatic - NO_x experiments with added CO, even though it has a slight tendency to overpredict O_3 in the aromatic - NO_x experiments
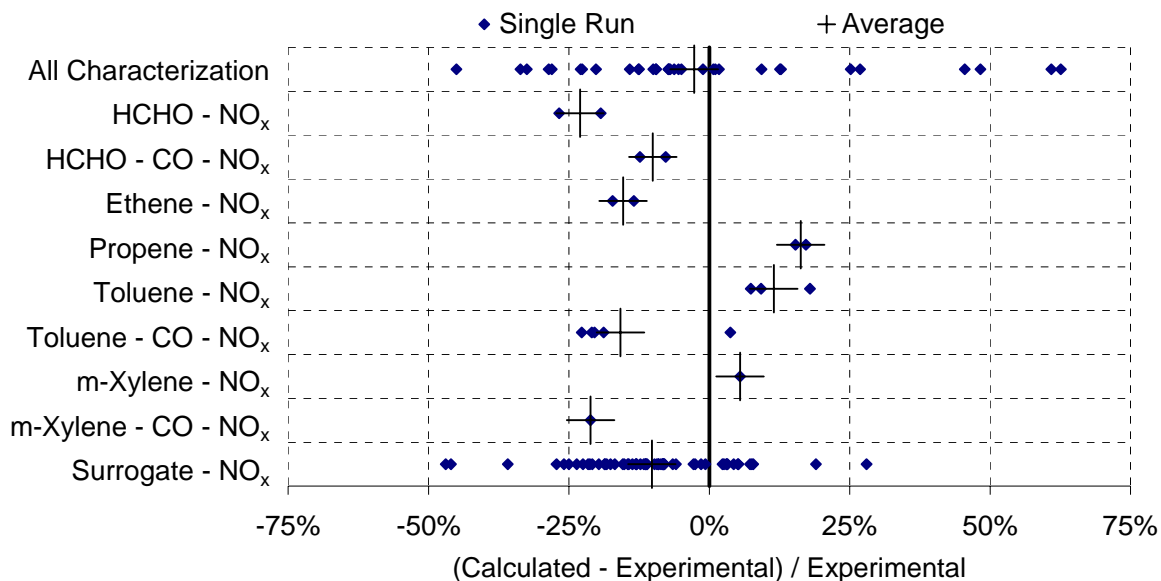
Figure 10. Fits of experimental O_3 formed and NO oxidized, $\Delta([O_3]-[NO])$, measurements to SAPRC-99 model calculations for the initial chamber and mechanism evaluation experiments.

without added CO. This suggests problems with the aromatics mechanisms that need further investigation (Carter, 2004).

The mechanism tended to have a bias towards underpredicting $\Delta([O_3]-[NO])$ in the ambient surrogate - NO_x experiments, though as indicated in Figure 10 this underprediction did not occur for all experiments. The underprediction bias had very little correlation with the initial ROG and NO_x levels in the experiments but was highly correlated with the initial ROG/NO_x ratio. This is shown in Figure 11, which gives plots of the $\Delta([O_3]-[NO])$ model underprediction bias against the initial ROG/NO_x ratio the experiments. The "error bars" show the effects of varying the HONO offgasing parameter over the extreme values shown in Figure 7 for this chamber for the 303±1 K temperature range, which applicable to these experiments. It can be seen that the model has a definite tendency to underpredict $\Delta([O_3]-[NO])$ at the low ROG/NO_x ratios. Although the HONO offgasing parameter has a non-negligible effect on the simulations of the experiments at the lowest and highest ROG/NO_x ratio (because of sensitivities to the radical source in the first case and to the NO_x source in the second), the sensitivity is not sufficient to account to the trend in the bias with ROG/NO_x. This trend was not evident in the previous mechanism evaluations, perhaps in part because of the greater variabilities of the model simulations due to greater chamber effects or characterization uncertainties, and perhaps in part because this is not as evident at higher reactant concentrations. This suggests problems with the mechanism that also needs further investigation (Carter, 2004).

As indicated in Table 3, the initial evaluation experiments included runs with NO_x levels as low as 2-5 ppb, which is considerably lower than in experiments used previously for mechanism evaluation. Most of the experiments used in the previous SAPRC-99 mechanism evaluation had NO_x levels greater than 50 ppb, and even the "low NO_x" TVA and CSIRO experiments had NO_x levels of ~20 ppb or greater, except for a few characterization runs (Carter, 2004, and references therein). However, other than the

27
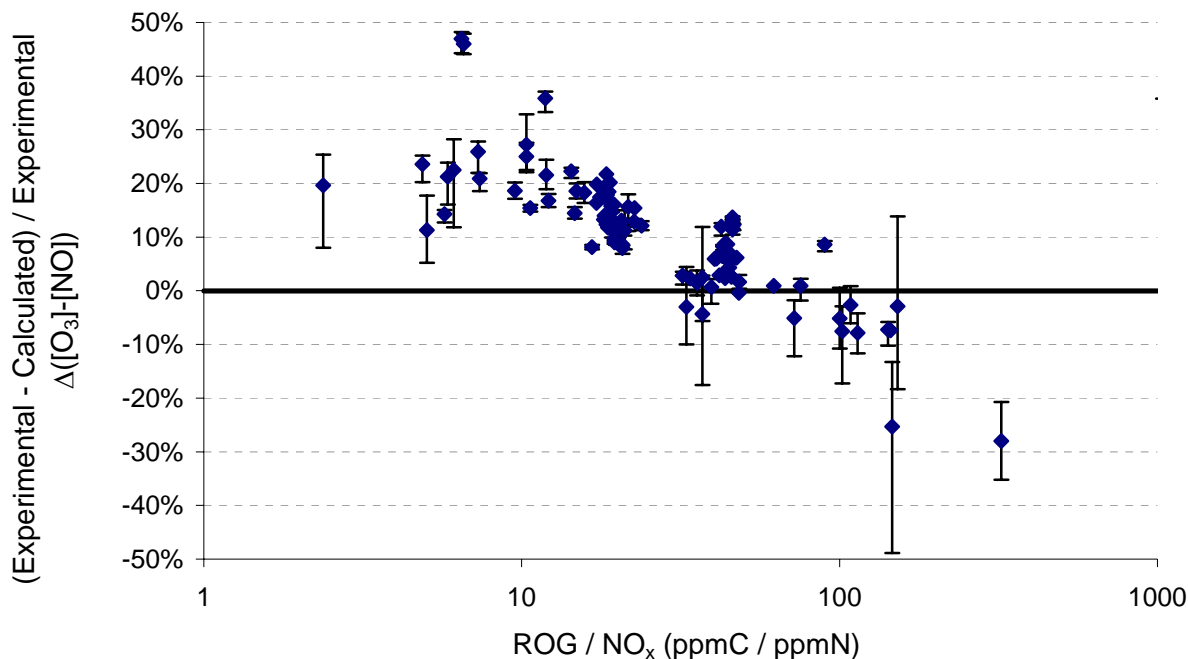
Figure 11.   Plots of the tendency of the SAPRC-99 mechanism for underpredicting ozone formed and NO oxidized, $\Delta([O_3]-[NO])$, against the initial ROG/NO$_x$ ratio in the surrogate - NO$_x$ experiments. Error bars show the effect of varying the HONO offgasing chamber effects parameter within its uncertainty.

ROG/NO$_x$ effect for the ambient surrogate experiments discussed above, there is no indication in any difference in model performance in simulating the results of these very low NO$_x$ experiments, compared to those with the higher NO$_x$ levels more representative of those used in the previous evaluation. This is an important finding because there has been a concern about using mechanisms evaluated at higher than ambient NO$_x$ levels for ambient simulations of remote areas or future case attainment scenarios (Dodge, 2000).

For example, Figure 12 shows concentration-time plots for selected measured species in ambient surrogate - NO$_x$ experiment carried out at the lowest NO$_x$ levels in the initial evaluation runs. To indicate the sensitivity of the experiments to NO$_x$ offgasing effects, the effects of varying the HONO offgasing parameter from zero to the maximum level consistent with the characterization experiments is also shown. It can be seen that the model using the default HONO offgasing parameter value gives very good fits to the data. Although the O$_3$ simulations are somewhat affected when the HONO offgasing rate is varied within this somewhat extreme range, the sensitivity is not so great that the uncertainty in this parameter significantly affects conclusions one can draw about the ability of the model to simulate this low NO$_x$ experiment. However, the sensitivity would increase as the NO$_x$ levels are reduced, and ~2 ppb NO$_x$ probably represents a reasonable lower limit for NO$_x$ levels useful for mechanism evaluation.

Overall, the results of the initial characterization and evaluation indicate that this chamber can provide high quality mechanism evaluation data for experiments with NO$_x$ levels as low as ~2 ppb, considerably lower than employed in previous experiments. Chamber effects are not absent, but they are as low or lower than in observed in any previous chambers used for mechanism evaluation, in some cases
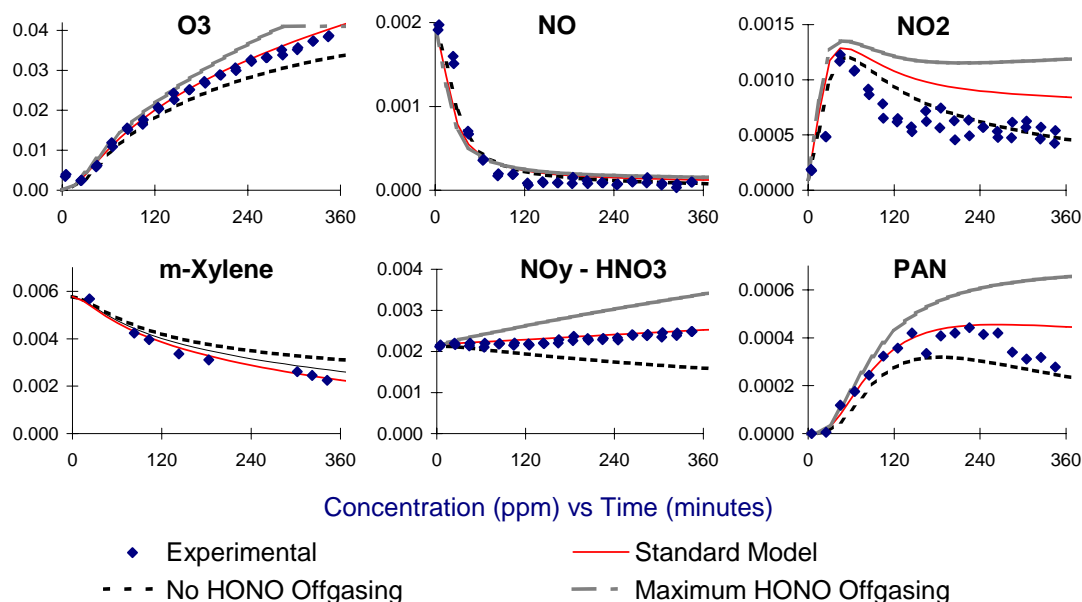
Figure 12.   Concentration-time plots of selected compounds in the lowest NO_x ambient ROG - NO_x surrogate experiment in the initial evaluation experiments ($NO_x \approx 1$ ppb, ROG ≈ 300 ppbC.

by an order of magnitude or more. Although a larger number of experiments would be required to fully assess this, the results also suggest a higher degree of precision in mechanism evaluation than observed previously, making smaller biases in mechanism performance more evident. The initial dataset from this chamber indicate no significant problems with mechanism performance that are characteristic of low NO_x conditions as such, but do reveal problems with the mechanisms for aromatics and the ambient ROG surrogate (Carter, 2004).

_m_-Xylene-NO_x SOA Yield

A series of m-xylene/NO_x experiments photooxidations were performed using the blacklights as an irradiation source. These blacklight experiments were carried with unhumidified air (dew point < -40 C), at atmospheric pressure (~740 torr local pressure) and at at 301±1 K. These experiments were used to determine our ability to perform SOA experiments. The data is analyzed following the original schemes outlined by Pankow et al. (1994a,b) and Odum et al. (1996). Briefly, SOA yield, Y, is defined as the ratio of aerosol ($\mu g\ m^{-3}$) to hydrocarbon reacted ($\mu g\ m^{-3}$).

$$Y = \sum_i Y_i = \Delta M_{org} \sum_i \frac{\alpha_i K_{om,i}}{1 + K_{om,i} \Delta M_{org}}$$

(2)

where α_i is the mass-based stoichiometric fraction of species i formed from the parent hydrocarbon, $K_{om,i}$ is the gas-particle partitioning coefficient ($m^3\ \mu g^{-1}$), which is inversely proportional to the compound's vapor pressure, and ΔM_{org} ($\mu g\ m^{-3}$) is the total mass concentration of organic material and associated water present in the aerosol phase. The fraction of secondary organic material condensing into the aerosol phase is seen to depend on the amount of organic aerosol mass present. The two-product semi-empirical

29

model then assumes that two surrogate species can be used to estimate the SOA yield: one surrogate product representing low vapor pressure compounds and one surrogate product representing high vapor pressure compounds. (i=1,2 in equation 2)

A set of characterization runs was carried out to demonstrate the ability of the chamber to perform SOA formation experiments. M-xylene was chosen as the initial test compound. Four experiments with initial m-xylene and NO initial concentrations of 75 ppb and 50 ppb respectively, T=300K, no initial aerosol present, and blacklight irradiation source were conducted until measurable aerosol volume growth (corrected for wall loss) had ceased (approximately 8 hours irradiation time, ~90% m-xylene consumption). The experiments were conducted on both reactors with a couple of months time separating the first and last experiment. Average total aerosol production for the four reactions was 21.4 ± 0.3 μg m^{-3}.

Additional *m*-xylene/NOx experiments were performed with blacklights for comparison to previously published yield data. The yield data are most easily compared to recent *m*-xylene irradiations at Caltech at comparable experimental conditions (indoors, blacklight source, similar temperatures) (Cocker et al. 2001c), and the results for the various chambers are shown on Figure 13. The "Empirical Fit through UCR Data" is the the best fit two product semi-empirical fit yield curve for the current dataset from this chamber, for which the parameters are 0.075, 0.105, 0.139, 0.010 for α_1, α_2, $K_{om,1}$, $K_{om,2}$, respectively. The overall agreement between this chamber and the Caltech chamber helps to verify the ability of the new chamber to accurately simulate gas-to-particle conversion processes. More details on the current dataset for *m*-xylene/NO$_x$ aerosol production can be found in Song et al. (2005).
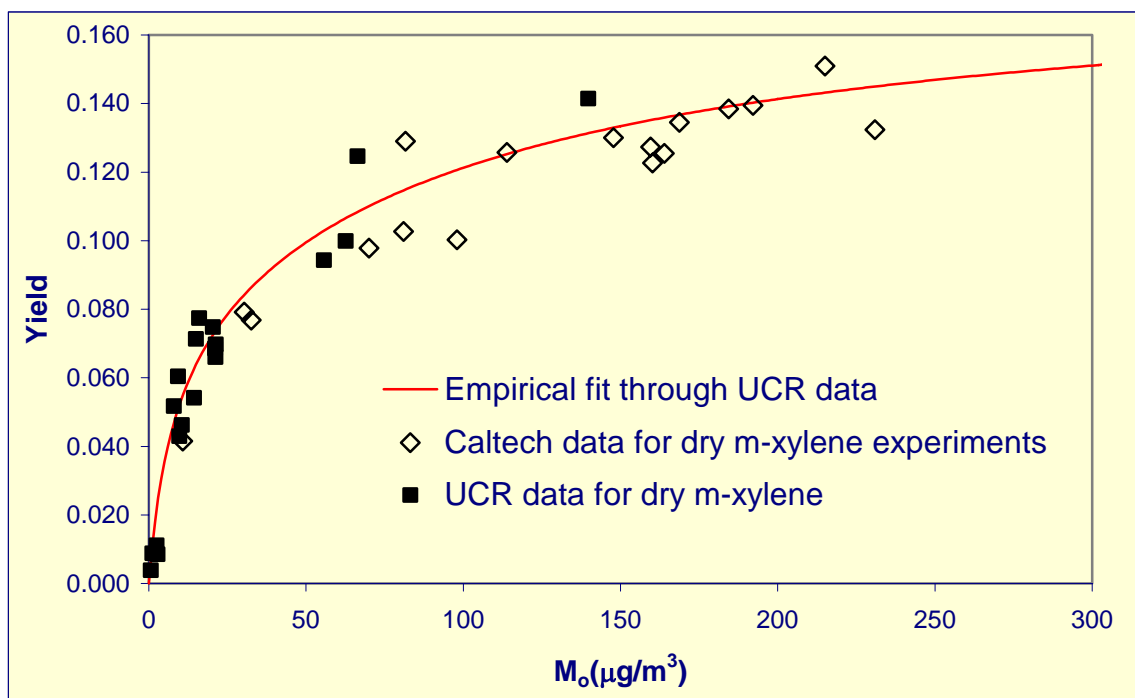

Figure 13. Comparison of yield data obtained for m-xylene/NOx system with blacklight irradiation. Solid squares represent data obtained in this reactor (UCR); open diamonds are for dry experiments conducted in the Caltech reactor (Cocker et al., 2001b); the solid line represents the best-fit two-product model for the current UCR data set.

DISCUSSION AND CONCLUSIONS

This chamber facility was designed to provide more precise and comprehensive mechanism evaluation data, and at lower simulated pollutant concentrations, than previously possible. Although the dataset from this chamber is still limited, the results to date demonstrate its utility for providing valuable data for mechanism evaluation. The major background effects parameters in the chamber appear to be lower than those observed in other chambers used for mechanism evaluation, including the TVA chamber, which was also designed for experiments at lower pollution levels (Simonaitis and Bailey, 1995; Simonaitis et al, 1997).

The lower background levels in this chamber permitted successful mechanism evaluation experiments to be carried out with NO_x levels as low as 2 ppb. This is at least an order of magnitude lower than in the mechanism evaluation dataset from other chambers used for gas-phase mechanism evaluation. In addition, we believe that the lower background effects attainable in this chamber provided an improvement in the precision of the mechanism evaluation dataset. The results of modeling the relatively large number of surrogate - NO_x experiments give some information regarding this. Although the model had systematic biases in simulating many of these experiments, as shown in Figure 11, plots of model biases against ROG/NO_x ratios had relatively little scatter, suggesting fits to within ±10% could be obtained if the current problem(s) with the mechanism can be corrected. This is less than the scatter for the fits to comparable experiments in other chambers (Carter and Lurmann, 1991; Carter, 2000, 2004). This is important since if the scatter in these fits were on the order of ±30%, which was observed mechanism evaluation studies using other chamber data sets (e.g., Carter and Lurmann, 1991), the ROG/NO_x dependences may not have been statistically significant, and the mechanism performance would have been concluded to be satisfactory. With this more precise dataset the low ROG/NO_x problem with the mechanism is evident.

We believe that this chamber is also well suited for studies of secondary aerosol formation. The good reproducibility of multiple experiments and general agreement with past work demonstrates our ability to accurately and precisely measure SOA formation potentials. Further work is clearly needed to characterize and eventually reduce or control background aerosol formation in this chamber, though this appears to be a problem with all environmental chambers used for aerosol studies. The relatively low chamber background effects and degree of characterization for gas-phase processes is also a significant advantage in studies of secondary PM formation, since it is the gas phase processes that lead to the formation of secondary PM. The ability to control temperature (and therefore humidity) is important, since data are needed to systematically study gas-to-particle conversion processes in well-controlled reactors.

Although the experiments reported here were carried only under dry conditions and at a single temperature, a humidification system has been constructed and the chamber is capable of controlled experiments in a wide temperature range of relevance to tropospheric pollution. Experiments to assess effects of varying humidity and temperature will be discussed in subsequent reports or papers.

REFERENCES

Bailey, E. M., C. H. Copeland and R. Simonaitis (1996): "Smog Chamber Studies at Low VOC and NOx Concentrations," Report on Interagency Agreement DW64936024 to EPA/NREL, Research Triangle Park, NC.

Barnes, I. and H. Sidebutton (2000). The European Photoreactor, 3rd report, 2000. Available at http://www.physchem.uni-wuppertal.de/PC-WWW_Site/pub/Projektberichte/EUPHORE _2000_final.pdf.

Brauers, T., B. Bohn, F.-J. Johnen, F. Rohrer, S. Rodriguez Bares, R. Tillmann, and A. Wahner (2003): "The Atmosphere Simulation Chamber SAPHIR: a Tool for the Investigation of Photochemistry," Presented at the EGS - AGU - EUG Joint Assembly, Nice, France, April 11, 2003. See also http://www.fz-juelich.de/icg/icg-ii/saphir/home.

Carter, W. P. L. (2000): "Documentation of the SAPRC-99 chemical mechanism for VOC reactivity assessment," Report to the California Air Resources Board, Contracts 92-329 and 95-308, May 8 (2000). Available at http://www.cert.ucr.edu/~carter/absts.htm #saprc99.

Carter, W. P. L. (2004): "Evaluation of a gas-phase atmospheric reaction mechanism for low NOx conditions," Final Report to California Air Resources Board Contract No. 01-305, May 5. Available at http://www.cert.ucr.edu/~carter/absts.htm#lnoxrpt.

Carter, W. P. L., R. Atkinson, A. M. Winer, and J. N. Pitts, Jr. (1982): "Experimental Investigation of Chamber-Dependent Radical Sources," Int. J. Chem. Kinet., 14, 1071.

Carter, W. P. L. and F. W. Lurmann (1991): "Evaluation of a Detailed Gas-Phase Atmospheric Reaction Mechanism using Environmental Chamber Data," Atm. Environ. 25A, 2771-2806.

Carter, W. P. L., and F. W. Lurmann (1990): "Evaluation of the RADM Gas-Phase Chemical Mechanism," Final Report, EPA-600/3-90-001.

Carter, W. P. L., D. Luo, I. L. Malkina, and D. Fitz (1995a): "The University of California, Riverside Environmental Chamber Data Base for Evaluating Oxidant Mechanism. Indoor Chamber Experiments through 1993," Report submitted to the U. S. Environmental Protection Agency, EPA/AREAL, Research Triangle Park, NC., March 20. Available at http://www.cert.ucr.edu/ ~carter/absts.htm#databas.

Carter, W. P. L., D. Luo, I. L. Malkina, and J. A. Pierce (1995b): "Environmental Chamber Studies of Atmospheric Reactivities of Volatile Organic Compounds. Effects of Varying Chamber and Light Source," Final report to National Renewable Energy Laboratory, Contract XZ-2-12075, Coordinating Research Council, Inc., Project M-9, California Air Resources Board, Contract A032-0692, and South Coast Air Quality Management District, Contract C91323, March 26. Available at http://www.cert.ucr.edu/~carter /absts.htm#explrept.

Carter, W. P. L., D. Luo, I. L. Malkina, and J. A. Pierce (1995c); "Environmental chamber studies of atmospheric reactivities of volatile organic compounds. Effects of varying ROG surrogate and NOx," Final report to Coordinating Research Council, Inc., Project ME-9, California Air Resources Board, Contract A032-0692, and South Coast Air Quality Management District, Contract C91323. March 24. Available at http:// www.cert.ucr.edu/~carter/absts.htm#rct2rept.

Carter, W. P. L. (2004): "Evaluation of a Gas-Phase Atmospheric Reaction Mechanism for Low NOx Conditions," Final report to the California Air Resources Board for Contract 01-305, May 5. Available at http://www.cert.ucr.edu/~carter/absts.htm#lnoxrpt

Cocker, D. R., R. C. Flagan, and J. H. Seinfeld. (2001a). "State-of-the-art chamber facility for studying atmospheric aerosol chemistry," Environ. Sci. Technol. 35, 2594-2601.

Cocker, D. R., S. L. Clegg, R. C. Flagan, and J. H. Seinfeld. (2001b). "The effect of water on gas-particle partitioning of secondary organic aerosol. Part I: alpha-pinene/ozone system," Atmos. Environ, 35, 6049-6072.

Cocker, D. R., B. T. Mader, M. Kalberer, R. C. Flagan, and J. H. Seinfeld (2001c). "The Effect of Water on Gas-Particle Partitioning of Secondary Organic Aerosol. II: m-Xylene and 1,3,5-Trimethylbenzene Photooxidation Systems," Atmos. Environ. 35, 6073-6085.

Collins D. R., R. C. Flagan, and J. H. Seinfeld (2001). Improved inversion of scanning DMA data. In press. Aerosol Science Technology

Dodge, M. C. (2000): "Chemical Oxidant Mechanisms for Air Quality Modeling, Critical Review Paper for 1998 Ozone Assessment," Atmos. Environ, 34, 2103-2130.

Gaffney, J. S, R. M. Bornick, Y-H Chen, and N. A. Marley (1998): "Capillary gas chromatographic analysis of nitrogen dioxide and PANs with luminol chemiluminescent detection," Atmos. Environ. 32, pp.1445-1454.

Gery, M. W., G. Z. Whitten, and J. P. Killus (1988): "Development and Testing of the CBM-IV For Urban and Regional Modeling," EPA-600/ 3-88-012, January.

Griffin, R. J., D. R. Cocker, J. H. Seinfeld, D. Dabdub (1999) "Estimate of global atmospheric organic aerosol from oxidation of biogenic hydrocarbons," Geophysical research letters 26 (17): 2721-2724.

Griffin, R. J., D. Dabdub M. J. Kleeman, M. P. Fraser, G. R. Cass, and J. H. Seinfeld (2002). "Secondary organic aerosol - 3. Urban/regional scale model of size- and composition-resolved aerosols," Journal of Geophysical Research-Atmospheres 107 (D17), Art. No. 4334.

Griffin, R. J., D. R. Cocker, R. C. Flagan, and J. H. Seinfeld (1999). "Organic aerosol formation from the oxidation of biogenic hydrocarbons," Journal of Geophysical Research-Atmospheres 104 (D3): 3555-3567.

Hastie, D. R, G. I. Mackay, T. Iguchi, B. A. Ridley, and H. I. Schiff (1983): "Tunable diode laser systems for measuring trace gases in tropospheric air," Environ. Sci. Technol. 17, 352A-364A.

Hess G. D., F. Carnovale. M. E., Cope. and G. M. Johnson (1992) "The evaluation of some photochemical smog reaction mechanisms – 1 temperature and initial composition effects", Atmos. Environ., 26A, 625-641.

Holdren, M. W. and C. W. Spicer (1984): "Field Compatible Calibration Procedure for Peroxyacetyl Nitrate," Environ. Sci. Technol., 18, 113-115.

Jacobsen, N. W. and R. G. Dickinson (1994): "Spectrometric Assay of Aldehydes as 6-Mercapto-3-substituted-s-triazolo(4,3-b)-s-tetrazines," Analytical Chemistry 46/2 (1974) 298–299.

Jang M. S. and R. M. Kamens (2001): "Characterization of secondary aerosol from the photooxidation of toluene in the presence of NOx and 1-propene," Environmental Science & Technology 35 (18): 3626-3639.

Jaoui M., K. G. Sexton, and R. M. Kamens (2004): "Reaction of alpha-cedrene with ozone: mechanism, gas and particulate products distribution," Atmospheric Environment 38 (17): 2709-2725.

Jeffries, H. E., R. M. Kamens, K. G. Sexton, and A. A. Gerhardt (1982): "Outdoor Smog Chamber Experiments to Test Photochemical Models", EPA-600/3-82-016a, April.

Jeffries, H. E., K. G. Sexton, R. M. Kamens, and M. S. Holleman (1985a): "Outdoor Smog Chamber Experiments to Test Photochemical Models: Phase II," Final Report, EPA-600/3-85-029.

Jeffries, H. E., K. G. Sexton, T. P. Morris, H. Jackson, R.G. Goodman, R. M. Kamens, and M. S. Holleman (1985b): "Outdoor Smog Chamber Experiments Using Automobile Exhaust," Final Report, EPA-600/3-85-032.

Jeffries, H. E., K. G. Sexton, and M. S. Holleman (1985c): "Outdoor Smog Chamber experiments: Reactivity of Methanol Exhaust", Final Report, EPA-600/3-85-009a, September

Jeffries, H. E., K. G. Sexton, J. R. Arnold, Y. Bei, J. L. Li, and R. Crouse (1990): "A Chamber and Modeling Study to Assess the Photochemistry of Formaldehyde," Report on EPA Cooperative Agreement 813964, Atmospheric Research and Exposure Assessment Laboratory, U.S. EPA, Research Triangle Park, NC.

Jeffries, H. E.; M. W. Gery, and W. P. L. Carter (1992) Protocol for evaluating oxidant mechanisms for urban and regional models. Report for U.S. Environmental Protection Agency Cooperative Agreement No. 815779, Atmospheric Research and Exposure Assessment Laboratory, Research Triangle Park, NC.

Johnson, D., Jenkin, M. E. Wirtz, K., and Montserrat, M-R (2004). "Simulating the formation of secondary organic aerosol from the photooxidation of toluene environmental chemistry," Environ. Chem. 1, 150-165

Kleindienst, T. E., D. F. Smith, W. Li, E. O. Edney, D. J. Driscoll, R. E. Speer R, and W. S. Weathers (1999). "Secondary organic aerosol formation from the oxidation of aromatic hydrocarbons in the presence of dry submicron ammonium sulfate aerosol," Atmospheric Environment 33 (22): 3669-3681.

Montserrat, M-R, Wirtz, K (2005). "Is benzene an precursor for secondary organic aerosol?" Environ. Sci. Technol. 39, 1045-1054

NIOSH (1994): "Sulfite titration of formaldehyde stock solution: modified Method 3500," NIOSH Manual of Analytical Methods, NMAM, fourth edition, August 15.

Odum J. R., T. Hoffmann, F. Bowmam, D. Collins, R, C, Flagan, and J. H. Seinfeld (1996). "Gas/particle partitioning and secondary organic aerosol yields," Environ. Sci. Technol. 30, 2580-2585.

Odum J. R., T. P. W. Jungkamp, R. J. Griffin, R. C. Flagan and J. H. Seinfeld (1997). "The atmospheric aerosol-forming potential of whole gasoline vapor," Science 276 (5309): 96-99.

Pandis, S.N., R, A. Harley, G. R. Cass, and J. H. Seinfeld (1992). "Secondary organic aerosol formation and transport," Atmospheric Environment, 26(13):2269-2282.

Pankow, J. F. (1994). "An absorption model of gas/particle partitioning of organic compounds in the atmosphere," Atmos. Environ. 28, 185-188.

Pankow, J. F. (1994), "An absorption model of the gas/aerosol partitioning involved in the formation of secondary organic aerosol," Atmos. Environ. 28, 189-193.

Pun B. K., S. Y. Wu, C. Seigneur, J. H. Seinfeld, R. J. Griffin, and S. N. Pandis (2003). "Uncertainties in modeling secondary organic aerosols: Three-dimensional modeling studies in Nashville/Western Tennessee," Environmental Science & Technology, 37 (16): 3647-3661.

Quesenberry, M. S. and Y. C. Lee (1996): "A Rapid Formaldehyde Assay Using Puprald Reagent: Application under Periodation Conditions," Analytical Biochemistry. 234, 50–55.

Rohrer, F., Bohn, B., Brauers, T., Brüning, D., Johnen, F. -J., Wahner, A. and Kleffmann, J. (2004). "Characterisation of the photolytic HONO-source in the atmosphere simulation chamber SAPHIR," Atmos. Chem. and Physics Disc., 4, 7881-7915

Seinfeld, J. H. and J. F. Pankow (2003). "Organic atmospheric particulate material," Annual review of Physical Chemistry 54: 121-140.

Schiff, H.. I., G. I. Mackay, and J. Bechara (1994): "The Use of Tunable Diode Laser Absorption Spectroscopy for Atmospheric Measurements", Res. Chem. Intermed. 20, 1994, pp 525-556.

Simonaitis, R. and E. M. Bailey (1995): "Smog Chamber Studies at Low VOC and NOx Concentrations: Phase I," Report on Interagency Agreement DW64936024 to EPA/NREL, Research Triangle Park, NC.

Simonaitis, R., J. Meagher, and E. M. Bailey (1997): "Evaluation of the condensed Carbon Bond Mechanism against smog chamber data at low VOC and NOx Concentrations," Atm. Environ. 31, 27-43

Song, C., K. Na, and D. R. Cocker (2005). "Impact of hydrocarbon to NOx ratio on secondary organic aerosol formation", Environ. Sci. and Technol., 39, 3143-3149.

Stockwell, W. R., P. Middleton, J. S. Chang and X. Tang (1990): "The RADM2 Chemical Mechanism for Regional Air Quality Modeling," J. Geophys. Res., 95, 16343-16367.

Wang, S. C. and R. C. Flagan (1990) Scanning Electrical Mobility Spectrometer. Aerosol Science and Technology. 13(2): 230-240 1990

Zafonte, L., P. L. Rieger, and J. R. Holmes (1977): "Nitrogen Dioxide Photolysis in the Los Angeles Atmosphere," Environ. Sci. Technol. 11, 483-487.